



RESEARCH ARTICLE

A multiscale approach to predict the binding mode of metallo beta-lactamase inhibitors

Silvia Gervasoni¹  | James Spencer²  | Philip Hinchliffe²  |
Alessandro Pedretti¹  | Franco Vairoletti³  | Graciela Mahler³  |
Adrian J. Mulholland⁴ 

¹Department of Pharmaceutical Sciences, University of Milan, Milan, Italy

²School of Cellular and Molecular Medicine, University of Bristol, Bristol, UK

³Facultad de Química, Departamento de Química Orgánica, Laboratorio de Química Farmacéutica, Universidad de la República (UdelaR), Montevideo, Uruguay

⁴School of Chemistry, University of Bristol, Bristol, UK

Correspondence

Adrian J. Mulholland, School of Chemistry, University of Bristol, Bristol, UK.
Email: adrian.mulholland@bristol.ac.uk

Funding information

Agencia Nacional de Investigación e Innovación, Grant/Award Numbers: ANII (POS_NAC_2018_1_151488), POS_NAC_2018_1_151488; Engineering and Physical Sciences Research Council, Grant/Award Numbers: EP/M022609/1, T016035/1, M022609/1; Medical Research Council, Grant/Award Number: MR/T016035/1; National Institutes of Health; National Institute of Allergy and Infectious Diseases, Grant/Award Number: R01AI100560; University of Bristol; Computing Research Centre

Abstract

Antibiotic resistance is a major threat to global public health. β -lactamases, which catalyze breakdown of β -lactam antibiotics, are a principal cause. Metallo β -lactamases (MBLs) represent a particular challenge because they hydrolyze almost all β -lactams and to date no MBL inhibitor has been approved for clinical use. Molecular simulations can aid drug discovery, for example, predicting inhibitor complexes, but empirical molecular mechanics (MM) methods often perform poorly for metalloproteins. Here we present a multiscale approach to model thiol inhibitor binding to IMP-1, a clinically important MBL containing two catalytic zinc ions, and predict the binding mode of a 2-mercaptomethyl thiazolidine (MMTZ) inhibitor. Inhibitors were first docked into the IMP-1 active site, testing different docking programs and scoring functions on multiple crystal structures. Complexes were then subjected to molecular dynamics (MD) simulations and subsequently refined through QM/MM optimization with a density functional theory (DFT) method, B3LYP/6-31G(d), increasing the accuracy of the method with successive steps. This workflow was tested on two IMP-1:MMTZ complexes, for which it reproduced crystallographically observed binding, and applied to predict the binding mode of a third MMTZ inhibitor for which a complex structure was crystallographically intractable. We also tested a 12-6-4 nonbonded interaction model in MD simulations and optimization with a SCC-DFTB QM/MM approach. The results show the limitations of empirical models for treating these systems and indicate the need for higher level calculations, for example, DFT/MM, for reliable structural predictions. This study demonstrates a reliable computational pipeline that can be applied to inhibitor design for MBLs and other zinc-metalloenzyme systems.

KEYWORDS

antibiotic resistance, IMP-1, MBL inhibitor, metallo β -lactamases, metalloenzymes, thiazolidine, zinc enzymes

This is an open access article under the terms of the Creative Commons Attribution License, which permits use, distribution and reproduction in any medium, provided the original work is properly cited.

© 2021 The Authors. *Proteins: Structure, Function, and Bioinformatics* published by Wiley Periodicals LLC.

1 | INTRODUCTION

The spread of antimicrobial resistance (AMR) threatens our capability to treat infectious disease.¹ Microorganisms have developed several resistance mechanisms including efflux pump production, target alteration, decreased drug uptake and drug inactivation.² The latter mechanism is one of the most important and is most often seen in the form of the hydrolysis of β -lactam antibiotics, catalyzed by serine- β -lactamases (SBLs) and metallo- β -lactamases (MBLs).^{3,4} One effective strategy to overcome this resistance mechanism is to inhibit β -lactamases.⁵⁻⁸ However, while for the SBLs several compounds of different classes have already been approved for clinical use, no MBL inhibitor has yet been approved.⁷

MBLs can be divided into three subclasses: B1, B2, and B3, with B1 as the most clinically significant because they catalyze the hydrolysis of a broad spectrum of β -lactams⁹ and several family members, notably the NDM, IMP and VIM enzymes, are disseminating among Gram-negative bacterial pathogens (e.g., *Escherichia coli*, *Pseudomonas aeruginosa*) on mobile genetic elements.^{4,10} MBLs contain two catalytic zinc ions within the active site which participate in the reaction mechanism by coordinating the substrate and activating a bound water/hydroxide molecule to undergo nucleophilic attack upon the carbonyl carbon of the scissile amide^{4,11-13} (Figure 1). Thus, efforts have been made to design inhibitors that coordinate one or both the zinc ions and compete with substrate for binding to the active site,¹¹ which could potentially be co-administered with β -lactams to restore their efficacy against MBL-producing strains.

In silico drug discovery to identify MBL inhibitors is more challenging than for SBLs because of the presence of zinc ions. Zinc ions possess d orbitals that participate in chemical bonding and, compared to s or p orbitals, have more complicated shapes. Furthermore, zinc ions can have multiple coordination numbers and different coordination geometries.¹⁵ In molecular mechanics (MM) approaches, metal ions are often represented only as point charges with van der Waals interactions.^{16,17} This simplistic representation cannot reproduce all the properties of zinc described above and consequently fails to

successfully model the dynamic and versatile nature of zinc coordination in many biological systems.¹⁸⁻²⁰

Over the years there has been significant effort to overcome these limitations by introducing alternative MM models to treat metal ions, including bonded models, nonbonded models, ligand field molecular mechanics, cationic dummy atoms or polarizable force fields. Bonded models add bonding potentials between the metal ions and ligands and can also include angles, torsions, electrostatic and van der Waals terms; drawbacks include the inability to model ligand exchange and dissociation, or changes in coordination.²⁰ The ligand field molecular mechanics model incorporates the ligand field stabilization energy directly into the potential energy expression of molecular mechanics.²¹ The cationic dummy atom model places additional virtual atoms around the ion to mimic a covalent bond.²² Polarizable force fields include terms to account for the polarization effect, but so far are computationally expensive.²³ Finally, in typical MM nonbonded approaches, interactions are evaluated by the sum of the Coulomb and Lennard-Jones terms (Equation 1).²⁴ However, this type of simple model tends to underestimate the strength of the coordination, and does not represent coordination geometry preferences and other electronic effects.²⁴ For this reason, other nonbonded interaction models have been proposed, such as the restrained nonbonded model or the LJ12-6-4 model (Equation 2), which has been tested for both Mg^{2+} ^{25,26} and Zn^{2+} ions^{27,28} and contains an r^{-4} term that is included to describe the ion-induced dipole interaction.²⁹

$$U_{ij}(r_{ij}) = \frac{e^2 Q_i Q_j}{r_{ij}} + \frac{C_{12}^{ij}}{r_{ij}^{12}} - \frac{C_6}{r_{ij}^6} \quad (1)$$

$$U_{ij}(r_{ij}) = \frac{e^2 Q_i Q_j}{r_{ij}} - \frac{C_4}{r_{ij}^4} + \frac{C_{12}^{ij}}{r_{ij}^{12}} - \frac{C_6}{r_{ij}^6} \quad (2)$$

In this study, we investigate the binding of inhibitors to imipenemase (IMP)-1, a B1 MBL that is frequently found on mobile genetic elements that facilitate its spread through bacteria.^{10,30-32} The primary host, *Pseudomonas aeruginosa*, is a Gram-negative

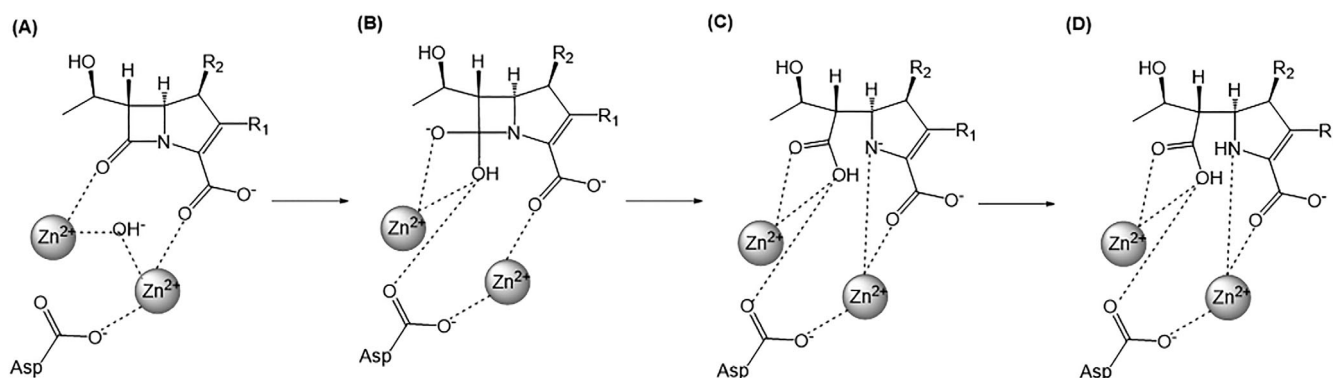


FIGURE 1 Possible mechanism of β -lactam ring hydrolysis by subclass B1 metallo- β -lactamases.¹²⁻¹⁴ (A) Reaction initiates with coordination of the zinc ions by the β -lactam (carbapenem shown here), with a hydroxide ion bridging the two metal ions. (B) The carbonyl carbon of the β -lactam ring undergoes nucleophilic attack by the hydroxide ion, leading to formation of a transient tetrahedral species; (C) cleavage of the C-N bond leads to the accumulation of an anionic intermediate; and (D) this may be resolved by protonation of the nitrogen

bacterial pathogen responsible for a variety of opportunistic infections of immunocompromised patients, and notably associated with infections of burn wounds and the lungs of individuals with cystic fibrosis.³³ In the continued absence of new antibacterial agents with anti-Gram-negative activity, infections by resistant *P. aeruginosa* strains are very difficult to treat.³⁴ Various compound classes have been investigated as potential MBL inhibitors (as reviewed^{4,7,9,11,35}); we here focus on thiol-containing compounds which exploit the high affinity of zinc for sulfur ligands and have been extensively investigated.^{36,37} In consequence, relatively extensive structural data exist for complexes of IMP-1 with thiol compounds that may be exploited for development and assessment of approaches to model inhibitor binding.^{36,38} Accordingly, we have developed a multiscale approach to investigate the binding of thiolate anions to IMP-1, in which successive docking, molecular dynamics (MD) and quantum mechanics/molecular mechanics (QM/MM) simulations provide for stepwise refinement of complex models. This has been applied to study a recently characterized series of 2-mercaptomethyl thiazolidine (MMTZ) inhibitors³⁹ (Figure 2), first successfully replicating two known crystal structures of IMP-1 complexes with two different MMTZs (D-*syn*-**1b** and L-*anti*-**1b**), and subsequently predicting the mode of binding for a third MMTZ (D-*anti*-**1a**) known to inhibit IMP-1 but for which the crystal structure of its complex with the protein could not be obtained. This approach could be applied to design other potential metallo- β -lactamase inhibitors to predict their binding mode and optimize their interactions with enzyme, aiding their development as potential pharmaceutical leads. Moreover, it could also be applied to model other similar metalloprotein systems: an example is represented by di-zinc metalloenzyme human carnosinase CN1, where Pavlin et al.⁴⁰ adopted a similar workflow (i.e., docking, MD and DFT/MM) to simulate the binding mode of the substrate carnosine.

2 | MATERIALS AND METHODS

2.1 | Molecular docking

Different docking procedures were tested for crystal structures of IMP-1 (see below) complexed with thiol-containing inhibitors (Figure S1) to find the docking setting that best reproduced their interactions. In each case the inhibitor was modeled and docked as its

thiolate anion. The region of the protein included in docking was selected by considering whole residues within a 10 Å radius around the two zinc ions of the IMP-1 active site, which comprises the whole catalytic pocket. Docking with PLANTS⁴¹ (see below) applied distance restraints between the sulfur atom of the ligand and the zinc ions with a weight of -7.5 kcal/mol, and a maximal and minimal distance of 3 and 1.30 Å, respectively. A σ value of 5 was applied to increase the number of search iterations of the ant colony optimization (ACO) algorithm⁴² and 10 000 clusters were produced, using the ChemPLP scoring function and the speed option equal to 1. Furthermore, we tested both the flexible (designated Opt1) and rigid (Opt2, Opt3) binding pocket, and we also included the water molecules present in the binding site of the crystal structures (Opt3). In Opt1 the side chains of Val31, Phe51, Lys161, Leu165, Asn167, Asp170, Trp176, and Ser198 (which face the binding site) were treated as flexible. For docking with AutoDock Vina, we considered the binding pocket as rigid and tested the procedure with and without crystallographic water molecules (Opt5 and Opt4, respectively). Other parameters used in the AutoDock Vina docking are given in the Supporting Information (Figure S2). The results of docking experiments were evaluated by computing RMSD values between binding poses identified by docking and the corresponding crystal structure.

2.2 | Molecular dynamics simulations

Amber 18⁴³ was used for MD simulations. Complexes derived from docking were solvated in a box of TIP3P water molecules, with 10 Å between the protein and the edges of the box. The systems were neutralized with Na⁺ and Cl⁻ ions at an ionic concentration of 0.15 M, and periodic boundary conditions were applied using the particle-mesh Ewald method for long range electrostatics. A cutoff of 8 Å was chosen for the evaluation of the nonbonded interactions. The energy output and the frames of the trajectories were printed every 2 ps. The ligands were prepared in Antechamber with AM1-BCC charges and GAFF as force field,⁴⁴ for which benchmarking in agreement with quantum calculation has been reported,⁴⁵ while the protein was parameterized using the ff14SB force field.⁴⁶ Given the challenges associated with evaluating the interactions between the zinc ions and their coordinating atoms, we tested two different nonbonded models. First, the restrained nonbonded model (LJ12-6-R), which combines a

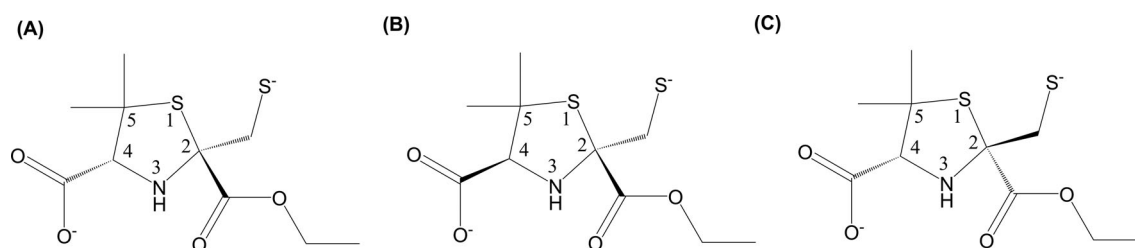


FIGURE 2 Structures of 2-mercaptomethylthiazolidine (MMTZ) inhibitors.³⁹ (A) D-*syn*-**1b**, (B) L-*anti*-**1b**, and (C) D-*anti*-**1a**. Note, the thiolate anion is drawn

TABLE 1 Distance restraints of the LJ12-6-R model

Residue number	Residue name	Atom name	Zinc ion	Distance
139	His	NE2	ZN1	2.1
77	His	NE2	ZN1	2.1
79	His	ND1	ZN1	2.0
81	Asp	OD2	ZN2	2.0
197	His	NE2	ZN2	2.1
158	Cys	SG	ZN2	2.3

Note: Equilibrium distances of the restrained nonbonded model between the zinc ions and the protein coordinating atoms are reported in Å.

nonbonded model (Equation 1) with distance restraints of 30 kcal/mol-Å between the two zinc ions and their coordinating protein atoms (Figure S3), and equilibrium distances as in the respective crystal structures (PDB ids 6ZYS for D-*syn-1b* and 6ZYR for L-*anti-1b*, respectively³⁹) (Table 1). Second, a 12-6-4 nonbonded model (LJ12-6-4) (Equation 2) in which an extra term is added to the Lennard-Jones equation²⁸ to represent the charge-induced dipole interaction, and for which no distance restraints were applied.

We applied the SHAKE algorithm⁴⁷ and a time step of 2 fs. The simulation protocol included energy minimization of the hydrogen atoms followed by minimization of the water molecules, and finally of the whole complexes, using 100 steps of steepest descent and 2900 steps of the conjugate gradient algorithm. The system was then heated to 300 K using the Langevin thermostat for 20 ps. Equilibration was performed at a pressure of 1 atm with the Berendsen barostat for 240 ps. Finally, we computed the production run using the NVT ensemble over 100 ns.

2.3 | QM/MM optimization

For QM/MM calculations we tested an approximate DFT-based method, SCC-DFTB (self-consistent charge-density functional tight binding, abbreviated here as DFTB, in particular DFTB3 that is a third order expansion of DFTB⁴⁸) and a DFT method.⁴⁹ The latter originates from the Kohn-Sham formulation. SCC-DFTB is in turn derived from DFT by approximation and parameterization of multi-center electron integrals, resulting in a significant increase in speed of calculation at the expense of accuracy.⁵⁰ SCC-DFTB/MM geometry optimization was performed with DFTB3 for the QM region and the ff14SB force field for the MM region using Amber. DFT QM/MM optimization was carried out using ChemShell,⁵¹ which combines MM and QM software: in detail, the MM portion of the system was handled by DL-Poly⁵² using the Amber ff14SB force field, while Gaussian09 handled the QM portion, with electrostatic embedding. In both DFT/MM and DFTB3/MM optimizations, the QM region was defined as the zinc ions, the ligand, any water molecule coordinated to the zinc ions, the side chains of the zinc coordinating residues (His77, His79, Asp81, His139, Cys158, Lys161, and His197), and the side chain of the conserved residue Lys161 that interacts with the ligands (Figure S4). In the DFT optimization, a

sphere of 8 Å around the QM region was considered as the active portion, while the remaining residues were fixed to decrease the computational cost. For the QM portion, we tested both the B3LYP and PBE0 hybrid functionals with the 6-31G(d) basis set and the DFT-D2 Grimme dispersion correction,⁵³ which can be important for predicting accurate structures.⁵⁴ We considered the zinc ions as closed shells. Covalent C-C bonds between the MM and the QM regions were capped with hydrogen atoms.

3 | RESULTS

3.1 | Method validation

We envisaged a workflow for developing models of IMP complexes with thiol-based inhibitors that involved successive steps (docking, MD, QM/MM), of higher levels of theory, to improve the accuracy of the final model. As described in Methods, for each step we tested multiple settings, in order to find the best combination to describe the structure and interactions with the metal ions.

We first tested docking options and scoring functions for thiolate anion-containing inhibitors (Table 1). Molecular docking predicts the binding mode of a ligand to a target molecule, usually a receptor or an enzyme. The resulting poses are generated by the combination of the conformational sampling algorithm, which explores the conformers of the ligand, and the scoring function that ranks those poses. When metal ions are included in the docking region, the scoring function needs to address a further level of complexity that can lead to the failure of the prediction of the correct binding mode.⁵⁵ We tested two docking tools that use two different search algorithms: the ant colony optimization (ACO) and the genetic algorithm (GA), namely PLANTS⁴⁵ and AutoDock Vina,⁵⁶ respectively. Moreover, these docking tools apply different scoring functions: ChemPLP from PLANTS derives from the combination of ChemScore and Piecewise Linear Potential (PLP) and includes a specific term to evaluate the coordination interaction,⁵⁷ while the AutoDock Vina Energy was calculated from the AutoDock4 scoring function and does not include specific terms for metal coordination.⁵⁶ Both these tools were tested with different settings in order to determine the setup that most reliably reproduced the crystal structures of protein-ligand complexes.

Literature and database searches identified crystal structures of IMP complexes with seven different thiols (Figure S1), to which we added our own recently determined structures of IMP complexes with two different MMTZ stereoisomers/diastereomers.³⁹ These nine thiol-based inhibitors were modeled as their thiolate anions and redocked into the corresponding (ligand-free) IMP-1 crystal structures using either PLANTS⁴⁵ or AutoDock Vina⁵⁶ and alternative treatments for the protein binding pocket, with the aim of obtaining an average ligand RMSD to the experimental crystal structure of <2 Å. Table 2 reports the RMSD values computed for the docking poses with the best score (i.e., lowest energy). RMSD values for the 20 best docking poses (numbered in order of increasing energy) for each docking protocol (from Opt1 to Opt5) are reported in Figure S5. While there is no clear correlation between RMSD values and energy/rank order of a specific pose, in general the first (lowest energy) pose is associated with RMSD values that are at or close to the lowest in the set. Our data (Table 2) show that using flexible side

chains in the binding pocket (Opt1) resulted in relatively high RMSD values (mean RMSD 4.47 Å). Indeed, lower RMSD values were generally obtained using a rigid binding pocket (Opt2, Opt4), and these further improved (for six out of nine thiolate ligands) when PLANTS was used with crystallographic water molecules added to the binding pocket (Opt3). This highlights the important role of interactions involving the water network in the binding sites of ligands.^{62–64} However, with one exception (PDB id: 2DOO⁶⁰), improvement was generally not observed when AutoDock Vina was used with water molecules included. Comparing the average RMSD values (2.74 Å) we identified the Opt3 approach as providing the best results, with six out of nine ligands reaching the target RMSD of <2 Å with respect to the crystal structure. Redocking of the mercaptopropionamide ligand to 2DOO was significantly worse, probably due to the large size and flexibility of the ligand compared to the others tested here, but also to the low resolution of the crystal structure, and it performed poorly in all the docking settings.

TABLE 2 RMSD values of the ligands between the crystal structure and redocked pose

IMP-1PDB Code	Resolution (Å)	Inhibitor	PLANTSOpt1 ^a	PLANTSOpt2 ^b	PLANTSOpt3 ^c	AutoDock VinaOpt4 ^d	AutoDock VinaOpt5 ^e
6ZYR ³⁹	1.87	MMTZ (L- <i>anti</i> -1b)	5.56	4.27	1.91	4.1	4.25
6ZYS ³⁹	1.87	MMTZ (D- <i>syn</i> -1b)	4.74	3.49	4.57	4.25	4.32
1DD6 ⁵⁸	2	Mercaptocarboxylate	9.46	2.34	1.7	4.17	4.58
1VGN ⁵⁹	2.63	Ethanethiolate	8.41	2.94	2.94	5.24	5.18
2DOO ⁶⁰	2.43	Mercaptopropionamide	4.39	4.3	7.68	11.08	5.1
4C1F ³⁸	2.01	L-captopril	2.13	5.18	1.18	3.91	3.91
4C1G ³⁸	1.71	D-captopril	2.01	2.07	1.73	4.46	4.46
5EV8 ⁶¹	2.3	D-bisthiazolidine	2.13	1.09	1.63	3.52	3.52
5EWA ⁶¹	2.3	L-bisthiazolidine	1.37	1.23	1.29	2.94	2.95
Mean RMSD			4.47	2.99	2.74	4.85	4.25
Mean RMSD excluding 2DOO			4.48	2.83	2.12	4.07	4.15

Note: All the RMSD values are reported in Å.

^aOpt1: S-Zn distance restraints, flexible binding pocket.

^bOpt2: S-Zn distance restraints, rigid binding pocket.

^cOpt3: S-Zn distance restraints, rigid binding pocket, crystallographic water molecules.

^dOpt4: rigid binding pocket.

^eOpt5: rigid binding pocket, crystallographic water molecules.

TABLE 3 Average RMSD (Å) between the crystal structures of L-*anti*-1b and D-*syn*-1b complexes, MD simulated (upper panel) and B3LYP/6-31G(d)/MM optimized complexes (lower panel)

		MD model	D- <i>syn</i> -1b	L- <i>anti</i> -1b
MD simulation	Binding-site ^a	LJ12-6-R	1.9 ± 0.7	1.8 ± 0.3
		LJ12-6-4	1.2 ± 0.3	1.6 ± 0.2
	Ligand	LJ12-6-R	1.1 ± 0.2	1.2 ± 0.2
		LJ12-6-4	1.2 ± 0.1	1.2 ± 0.1
QM/MM optimization	Binding-site ^a	From LJ12-6-R	1.3	1.2
		From LJ12-6-4	1.2	1.4
	Ligand	From LJ12-6-R	0.7	1.4
		From LJ12-6-4	1.1	1.3

^aBinding site residues: Glu23, Val25, Trp28, Val31, Phe51, Ala53, His77, His79, Ser80, Asp81, His139, Thr140, Cys158, Lys161, Gly166, Asn167, Ser196, His197, HO⁻, ZN1, ZN2.

The results of the best docking runs (Opt3) for the two MMTZ compounds for which complex structures were available were then subjected to molecular dynamics (MD) simulations to improve the quality of the models obtained. These were run using either the restrained nonbonded (LJ12-6-R) model or the LJ12-6-4 model; averaged RMSD values for the production run frames are reported in Table 3. In the two MD simulations the average RMSD values (compared to crystal structures) of the binding site residues for the LJ12-6-4 model are consistently lower than those for the LJ12-6-R, although in the latter the inhibitor RMSD is slightly smaller, suggesting slightly greater stability of the complex. In general, for both treatments, the difference in coordination bond lengths compared to the crystal structure is small (Figure 3).

In the crystal structures of both MMTZ complexes the two zinc ions are each in a tetrahedral geometry, with the first (ZN1) coordinated by three histidine residues (His77, His79, His139) and by the thiol moiety of the inhibitor, while the second (ZN2) is coordinated by Cys158, Asp81, His197, and by the inhibitor thiol, which, as in other crystallographic complexes of IMP-1 with thiol-based inhibitors,³⁶ replaces the zinc-bridging hydroxide present in unliganded structures.⁶⁵ However, during MD simulations using either model, the coordination number of the zinc ions tends to increase, through addition of extra water molecules, up to a limit of six. This tendency is enhanced when the LJ12-6-4 model is used. It is worth noting that in general the distance between the two zinc ions did not change significantly (i.e., the largest difference was 0.77 Å, found in the L-*anti*-1b LJ12-6-4 simulation).

Finally, we refined the inhibitor complex models with QM/MM geometry optimization. In the refinement step we tried two different methods: DFTB3 and DFT, and in the latter tested two functionals (B3LYP and PBE0). The DFTB3/MM method was tested to establish whether it could improve structures from MM MD (e.g., whether it would decrease the RMSD and recover the tetrahedral geometry of the zinc ions that was observed in the crystal structures). Thus, the complexes underwent a DFTB3/MM geometry optimization. We

found no or only slight improvement in RMSD values (a decrease of 0.43 Å in the RMSD of the binding site in D-*syn*-1b) (Table S1, Figure S6), but the geometry of the zinc ions was not recovered: they remained octahedrally coordinated (Figure S7), even if DFTB3 was parameterized considering tetrahedral zinc-proteins as well.⁶⁶ Accordingly, DFTB3/MM was applied for other zinc tetrahedral complexes, but with further refinement with DFT.⁶⁷

DFT methods were then employed to provide a more accurate description of the metal ions, with application of the hybrid functionals B3LYP and PBE0 which are commonly used in QM/MM studies of zinc-containing proteins.^{68–70} Both functionals gave similar results: there are only very small differences between calculations carried out with the two functionals (Tables 3 and S1). We present the results obtained with the B3LYP/MM treatment. Final RMSD values, with respect to the experimental crystal structures, are reported in Table 3. Compared to MD treatments, with QM/MM optimization the RMSD values decreased, in particular when starting from the last frame of the LJ12-6-R MD simulation. Moreover, in this case, the zinc coordination distances after DFT/MM optimization are almost identical to those measured in the crystal structure (Figure 4) and the additional zinc-coordinating water molecules that were introduced during MD simulations moved away from the zinc ion, with the result that the starting (crystallographic) coordination geometry was restored. In contrast, in DFT/MM calculations starting from the last frame of the MD simulation using the LJ12-6-4 model, the zinc ions remain in the octahedral geometry. The distance between the two zinc ions also changed significantly using the LJ12-6-4 model, and the QM/MM optimization was unable to relocate the two ions at the correct separation distance. This demonstrates the need to apply restraints in MM MD simulations to maintain active site structure and metal ion coordination.

The results indicate that QM/MM optimization of MD simulations, carried out using the LJ12-6-R model, leads to restoration of the inhibitor binding mode observed in the crystal structure, with correct coordination geometry of the zinc ions. This approach

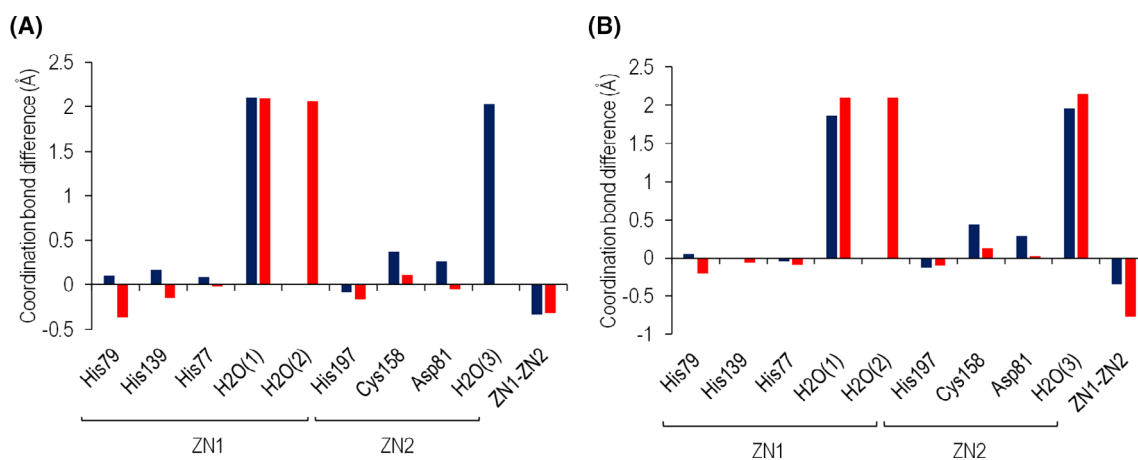


FIGURE 3 Comparison of coordination distances for crystal and MD-simulated structures (last frames) using the LJ12-6-R (blue) and LJ12-6-4 (red) models. Panel A refers to the D-*syn*-1b complex, panel B to the L-*anti*-1b complex. Water molecules that coordinate the zinc ions are also reported

successfully replicates the crystallographically observed binding modes of both *D-syn-1b* and *L-anti-1b*.

3.2 | Prediction of *D-anti-1a* MMTZ inhibitor binding mode to IMP-1

Previous study identified that a range of MMTZs,³⁹ including, but not limited to, *D-syn-1b* and *L-anti-1b*, act as micromolar inhibitors of IMP-1. However, in some cases crystal structures of inhibitor complexes with IMP-1 could not be obtained, even though biochemical data indicated that potency was comparable to that of compounds whose IMP-1 complexes could be structurally characterized. Accordingly, we sought to apply the approach developed here to model

interactions of an additional MMTZ inhibitor, *D-anti-1a*, with IMP-1. *D-anti-1a* is, respectively, a diastereoisomer and enantiomer of *D-syn-1b* and *L-anti-1b*. As it was unclear which of these complexes was likely to better accommodate the binding of *D-anti-1a*, docking experiments were carried out using IMP-1 conformations derived from both the *D-syn-1b* and *L-anti-1b* crystal structures, and subsequent simulations were undertaken in parallel.

Based upon the results above, molecular docking of *D-anti-1a* into IMP-1 in both conformations (i.e., from the *D-syn-1b* and *L-anti-1b* complexes) used the Opt3 approach described above. Figure 5 shows the binding modes obtained using the two crystal structures. The orientations of the *D-anti-1a* ligand differ significantly between the two models, with the inhibitor carboxylate group oriented towards the Lys161 side chain in the model based upon the *D-syn-1b* structure

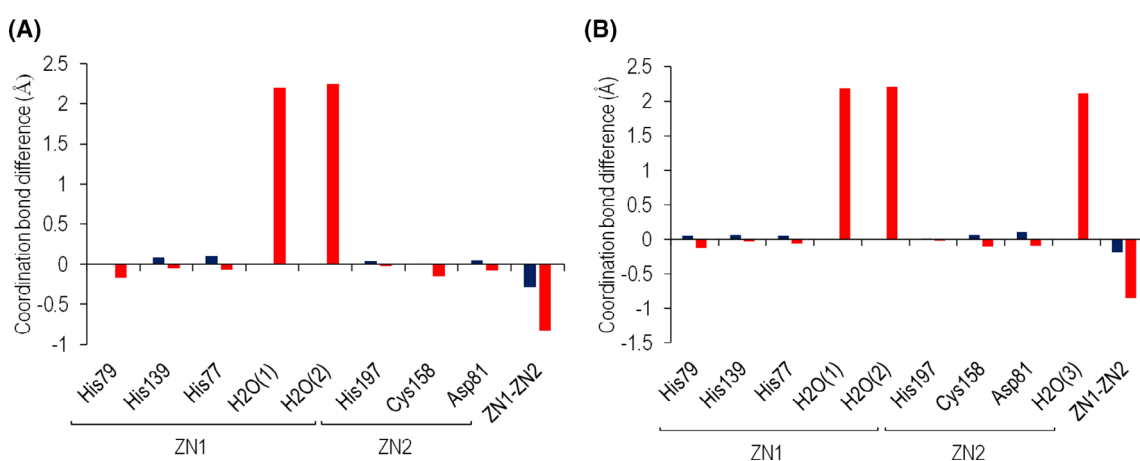


FIGURE 4 Differences in coordination bond length between crystal structures and B3LYP/6-31G(d) QM/MM optimized complexes. QM/MM optimization started from the last frame of MD simulations using the LJ12-6-R (blue) and the LJ12-6-4 (red) models. A *D-syn-1b* complex, B *L-anti-1b* complex. Water molecules coordinating the zinc ions are also reported

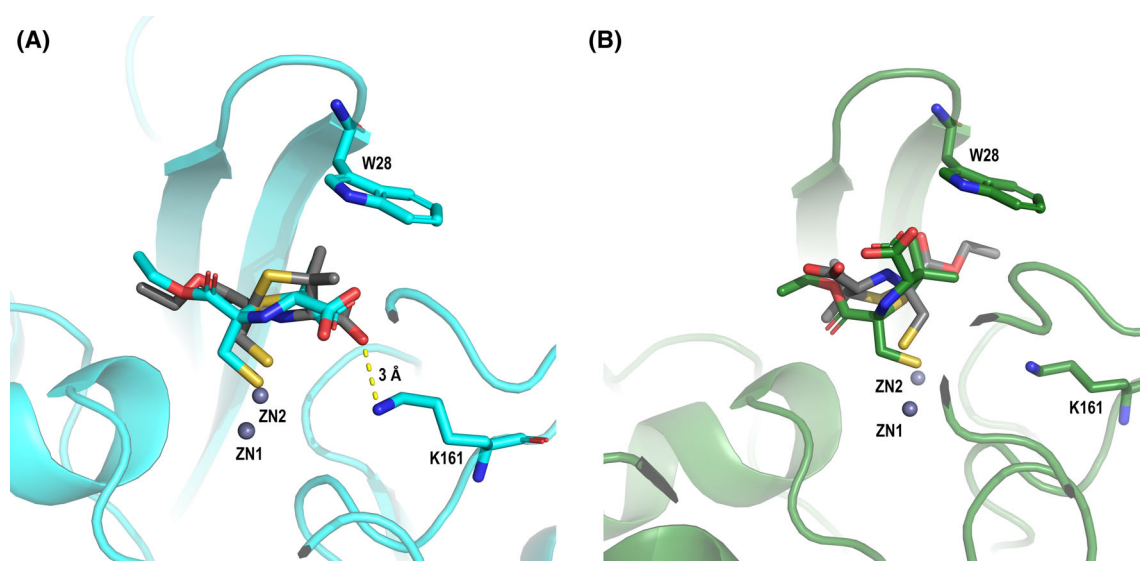


FIGURE 5 Superimposition of docked poses of the MMTZ inhibitor *D-anti-1a* (gray) on MMTZ complex crystal structures. (A) Docked *D-anti-1a* (gray) overlaid on *D-syn-1b* crystal structure (cyan). (B) Docked *D-anti-1a* (gray) overlaid on *L-anti-1b* crystal structure (green). Ligands are represented as sticks. The interaction between the ligand carboxylate group and Lys161 is highlighted with a dotted line

(with a distance of 3 Å between the carboxylate group and the lysine amino group), while in that based upon the L-*anti-1b* structure the inhibitor thiazolidine core is reorientated $\sim 180^\circ$ compared to crystal structures and the interaction with Lys161 is lost. Therefore, further simulations tested which of the two conformations generated stable binding of the inhibitor to the IMP-1 active site.

To this end, we analyzed MD simulations on both the modeled structures using both the LJ12-6-R and LJ12-6-4 models. The averaged RMSD values of the binding site of all the MD frames are reported in Table 4. We obtained higher RMSD values (of both the ligand and the binding site) when docking was based on the L-*anti-1b* structure, suggesting that, in this structure, the protein was not in the optimal conformation to accommodate and establish interactions with D-*anti-1a*. In contrast, when based on the D-*syn-1b* structure, lower RMSD values of the binding site were obtained and the ligand remained more stable, with an RMSD along the trajectory that fluctuated around 0.5 Å (Figure S8). These values were little changed after QM/MM optimization using the B3LYP hybrid functional with the 6-31G(d) basis set (Table 4). Inspection of coordination distances (Table S2) showed that interactions of the inhibitor thiolate anion with both zinc ions were maintained under the different simulation conditions, with the exception of simulations starting from the L-*anti-1b* complex structure using the LJ12-6-R model, where coordination of ZN1 was lost after QM/MM treatment.

As observed for the simulations described above, the use of the LJ12-6-4 model resulted in increased coordination numbers for the active site zinc ions, and B3LYP/6-31G(d)/MM optimization did not restore the tetrahedral coordination geometry present in the crystal structures of either the D-*syn-1b* or L-*anti-1b* complexes. Figure 6 illustrates the differences in the coordination bond lengths with respect to the starting crystal structures in simulations using the LJ12-6-R model. During MD simulations based upon both starting structures an additional water molecule (H2O(1) in Figure 6) coordinates the first zinc ion, changing the original tetrahedral coordination into pentahedral geometry. Moreover, in simulations based upon the L-*anti-1b* structure, residue Asp81 moved from the starting position and coordinated both zinc ions, which contrasts with the architecture reported in published crystal structures of IMP-1 and its complexes.^{38,58–61} Notably, however, after QM/MM optimization of simulations starting from the D-*syn-1b* structure, the additional water molecule (H2O(1)) that coordinated ZN1 moved away (from 2.1 to 2.5 Å, where we did not consider it to be coordinated), restoring the tetrahedral geometry of ZN1. In contrast, in simulations starting from the L-*anti-1b* structure, both the additional water molecule (H2O(1)) and Asp81 maintained coordination with ZN1 even after the QM/MM optimization. These results suggest that the structure of the complex obtained from simulations based upon the L-*anti-1b* structure is

TABLE 4 RMSD values of the D-*anti-1a* ligand binding site (Å) compared to L-*anti-1b* and D-*syn-1b* crystal structures

	MD model	D- <i>syn-1b</i> crystal structure	L- <i>anti-1b</i> crystal structure
MD simulation	LJ12-6-R	1.2 ± 0.2	2.2 ± 0.6
	LJ12-6-4	1.4 ± 0.2	1.5 ± 0.1
QM/MM optimization	From LJ12-6-R	1.3	2.6
	From LJ12-6-4	1.5	1.7

Note: Values were averaged from all frames of MD simulations (upper rows) and the B3LYP/6-31G(d)/MM optimized complexes (lower rows) using the LJ12-6-R and LJ12-6-4 models as indicated.

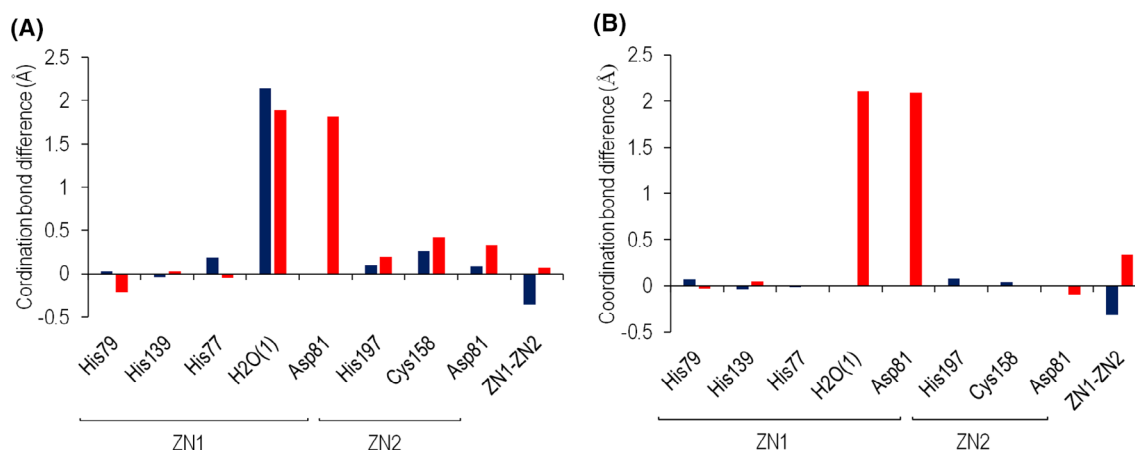


FIGURE 6 Differences in coordination bond lengths between crystal structures and modeled complexes of D-*anti-1b*. Values for models based upon L-*anti-1b* structure shown in red, values for models based upon D-*syn-1b* structure are shown in blue. (A) models derived from last frame of the LJ12-6-R MD simulation and (B) models derived from the B3LYP/6-31G(d) QM/MM optimization. H2O(1) is the additional water molecule that coordinates ZN1 (see text)

unlikely to be reliable, given the major changes in the coordination sphere of the metal center. On the other hand, the final complex derived from simulations based upon the *D-syn-1b* structure is consistent with crystallographically determined coordination distances and geometries for complexes of zinc metalloproteins and other thiol inhibitors reported in the literature.¹⁵

Given these data, we considered the final reliable model for *D-anti-1a* binding to be the complex obtained by using the *D-syn-1b* structure as the initial template, in which the inhibitor was docked using the Opt3 treatment, and subsequent MD simulation using the LJ12-6-R model and finally B3LYP QM/MM optimization.

The final predicted binding mode for the MMTZ inhibitor *D-anti-1a* is illustrated in Figure 7, with the thiolate anion coordinating both zinc ions. Notably, the conformation of Trp28 is changed, compared to its position in the crystal structure of the *D-syn-1b* complex. Conformational flexibility of this residue and the extended loop (sometimes termed the L3 loop) upon which it sits, has been previously described in multiple studies.^{61,71-73} Furthermore, there is significant movement away from the MMTZ of residues 165-172, part of loop L10⁷⁴ which forms the active site wall with loop L3. This contains Asn167 which weakly interacts with the MMTZ carboxylate in the *D-syn-1b* crystal structure. Here this interaction is lost, with *D-anti-1a* instead stabilized through interaction of this carboxylate with the amino group of the Lys161 side chain, that is also part of loop L10.

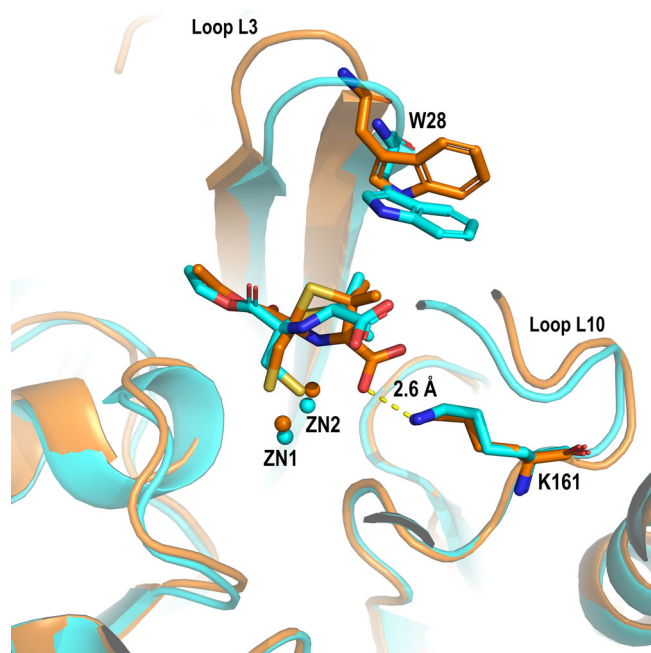


FIGURE 7 Superimposition of the modeled complex of IMP-1 with *D-anti-1a* on the crystal structure of the IMP-1 *D-syn-1b* complex. *D-anti-1a* and *D-syn-1b* complexes are shown in orange and cyan, respectively, ligands and interacting residues in sticks, and zinc ions as spheres. The *D-anti-1a* complex shown is obtained after QM/MM optimization. The interaction between the *D-anti-1a* carboxylate group and Lys161 is highlighted with a dotted line. Note, the thiazolidine rings lie perpendicular to each other, resulting in loss of the $S-\pi$ interaction with Phe51 in the *D-anti-1a* complex

During the MD simulation rearrangement of the loop L3, which contains Trp28, is observed, as well as of loop L10. This flexibility has been described in other studies and is consistent with the experimental evidence. However, in contrast to the behavior of these loops, the binding site of the enzyme remained stable for the entire trajectory, with average RMSD values below 2 Å. This is clearly evident from inspection of the RMSF values for these systems (Figure S9) in which high RMSF values were obtained for loop L3 (residues 21-32) and loop L10 (residues 162-172), while low values were obtained for the binding site (residues: Phe51, His77, His79, Ser80, Asp81, His139, Thr140, Cys158, Ser196, His197).

4 | DISCUSSION

The drug discovery process often relies upon molecular docking and MD simulations, which can usefully be combined.⁷⁵⁻⁷⁷ However, when considering metalloproteins, docking approaches suffer from important limitations due to the functional forms used to describe interactions of metal ions and related difficulties in their interactions, for which, for example, polarization is important.⁷⁸ It is well known that scoring functions struggle to correctly rank docking poses in metalloproteins.^{79,80} Similarly, despite several efforts to develop non-bonded parameters for metal ions,^{81,82} MD simulations with typical empirical MM forcefields also often fail to maintain protein-ligand complexes with correct metal ion coordination numbers and geometries.^{24,28,83} We found that the LJ12-6-4 nonbonded model led to changes from the original tetrahedral coordination into an octahedral geometry through addition of water molecules to the coordination spheres of both zinc ions. This incorrect coordination could not be reversed, even with QM/MM calculations. This variability of coordination geometry, which is an important contributor to the versatility and biological activity of metalloprotein zinc centers, thus compromises the stability of models of the binding site, and the reliability of predictions of ligand binding. In this study, we tested workflows to predict the binding mode of thiolate anion-containing inhibitors to metallo- β -lactamases, in which the accuracy of the method increases with the application of MD simulations followed by QM/MM modeling, and tested its ability to reproduce inhibitor binding modes seen in crystal structures. The overall approach has potential for application to drug discovery/design for zinc-containing proteins.

The best docking results were achieved by including the crystallographic water molecules, considering the protein as rigid and increasing the contribution of the interaction of the thiolate anion with the zinc ions, through addition of distance restraints to the ChemPLP scoring function.⁸⁴ This approach underlines the difficulty in producing docking poses in good agreement with experimental structures for these metalloenzymes. Empirical forcefields, current docking methods and even approximate quantum chemical methods fail to provide accurate structural predictions. It is because of these limitations that a rigid active site has to be used for reliable predictions. Inclusion of water molecules is also important. Our aim here was to test current methods and suggest practical routes to predict the structures of

bound complexes. While fully flexible docking would, in principle, be preferable, in practice it produces poor structures, because of the failings of currently available approximate methods. An additional consideration is the continuing challenge of accurately scoring docked structures, with none of the five approaches tested here readily differentiating between docked poses that more or less accurately reproduce the target crystal structures. However, the approach presented here was able to successfully reproduce crystal structures of our two test MMTZ inhibitors, even when, as in the case of *D-syn-1b*, the RMSD of the initial docked structure was relatively high. Docking methods alone cannot be used reliably to predict structures of bound metalloenzyme structures. Our conclusion is that, at present, reliable prediction of structures is only possible with density functional or high-level ab initio calculations, for example, in a combined quantum mechanics/molecular mechanics (QM/MM) framework.

MD simulations were used as a first step in refining the docked poses, with the lowest RMSD values observed using a restrained non-bonded model. As in docking experiments, restraints were necessary in MD simulations to maintain active site structure, demonstrating the limitations of empirical forcefields for modeling zinc sites. In MD, restraints were applied to the coordination distances between each zinc ion and the coordinating protein atoms. These MD simulations produced protein-ligand complexes in which the coordination number of the zinc ions still increased compared to crystal structures, though to a lesser extent in simulations using the LJ12-6-R as opposed to the LJ12-6-4 model because of the restraints added in the former. Further QM/MM calculations showed that the approximate SCC-DFTB3 method was unable to restore the experimentally observed coordination geometries of the metal ions, while use of more accurate DFT methods (i.e., B3LYP/6-31G(d)) enabled recovery of the tetrahedral geometries of the zinc ions present in the crystal structures as well as a significant reduction in RMSD. Our results thus demonstrate that this last step is of particular importance in obtaining correct coordination geometries that cannot be maintained using solely MM MD simulations. QM/MM optimization, with reasonable levels of DFT QM treatment, is required to generate reliable geometries for these complexes. The parameterization of the ligand is a further crucial point. In this study, the ligand was parameterized using Antechamber with AM1-BCC charges and GAFF as the force field, which is a standard and well tested approach. The methodological limitations of empirical forcefields, and of approximate DFTB methods, which our results highlight, mean that different molecular mechanics parameters for the ligands are not expected to improve performance overall. For predicting structures of metalloprotein complexes in general, there is a need for methods capable of the accuracy of good quality density functional or ab initio methods, but with significantly reduced computational cost, to allow for extensive docking of large numbers of compounds, conformational sampling and simulation. Machine learning from experimental data and quantum chemistry calculations, is a promising approach for developing empirical potentials and other computationally cheap models, that combine efficiency with accuracy.

In this study, we used RMSD values between the experimental structures of the protein complexes and the modeled ones (obtained

with the combination of docking, MD simulation and QM/MM optimization) as a measure of the error/agreement with experiment. High RMSD values (i.e., above 2–2.5 Å⁸⁵) are clear signs of errors in the structure of the simulated system. At this high RMSD level, the model should not be considered as being predictive. Here, the final RMSD values are below 2 Å in the binding site, which is the region of interest. This indicates that the error in the final structure is low and that the approach is reasonable and suitable for application to simulate similar systems. However, we would also stress that, for zinc (and other metal) centers such as those explored here, RMSD values alone do not provide a sufficient criterion for accuracy (although they can be sufficient to demonstrate failure of a method) and, as detailed above, nonphysiological geometries such as octahedral zinc coordination and/or adoption of metal-bridging by Asp81 can occur even when overall RMSD values are low. These factors should be considered in general in assessing the quality of predicted zinc metalloprotein complexes.

Notwithstanding these considerations, our workflow (Figure S10) produced a model for an inhibitor complex that is biochemically realistic both with respect to zinc coordination and interactions with active site residues (Lys161) known to be important to ligand binding by IMP-1.^{61,86,87} Involvement of Lys161 in our model of *D-anti-1a* binding by IMP-1 is notable given that such interactions are not observed in the crystal structures of either the *D-syn-1b* or *L-anti-1b* complexes. We have proposed that S- π interactions involving the thiazolidine ring sulfur and conserved aromatic residues at position 51 contribute to the affinity of MMTZs for subclass B1 MBLs such as IMP-1.³⁹ However, the displacement of Trp28 and reorientation of the MMTZ thiazolidine observed in our model suggests that these may not be maintained in the IMP-1:*D-anti-1a* complex. In this case, the loss of S- π interactions is then compensated for by the addition of a hydrogen bond to Lys161, ensuring that comparable inhibition potency is retained.³⁹

5 | CONCLUSIONS

In this study, we tested several techniques and their ability to reproduce inhibitor binding modes observed in crystal structures. However, we also identified methods that failed to correctly handle the metal coordination sphere. In detail, docking without the inclusion of crystallographic water molecules was not able to produce ligand binding poses with RMSD values lower than 2 Å compared with the corresponding original crystal structure. The results also demonstrate the limitations of standard MM models for MD simulations of these systems. In particular, MD simulations using a LJ12-6-4 model increased the coordination number of the zinc ions to six; this model may be well suited for use with zinc sites with octahedral coordination geometry,^{25,88} but appears less so for other architectures. Application of coordination restraints with a standard LJ12-6 model gave better results. Finally, we could not obtain the correct coordination geometry for the zinc ions when complexes from MD simulations were subjected to geometry optimization with the semi-empirical SCC-DFTB3/MM method. In contrast,

QM/MM geometry optimization with DFT methods restored the experimentally observed coordination. The results indicate the need for a high level/quantum chemical treatment for accurate modeling of zinc metalloenzyme active sites and their interactions, and demonstrate that such treatments can restore coordination geometries that may have been modified by previous procedures such as docking and/or MM treatments. Finally, we applied the workflow to predict the binding mode for an MMTZ MBL inhibitor for which the crystal structure of the complex with IMP-1 could not be obtained.

In summary, this study presents a validated, multiscale approach for the computational prediction of IMP-1 interactions with thiolate inhibitors. This approach is also suitable for application to studies of other MBL inhibitors, and other zinc-containing proteins.

ACKNOWLEDGMENTS

This study was carried out using the computational facilities of the Advanced Computing Research Centre, University of Bristol—<http://www.bris.ac.uk/acrc/>. This study was supported by the National Institute of Allergy and Infectious Diseases of the National Institutes of Health (NIH) to James Spencer and Graciela Mahler under Award Number R01AI100560. The content is solely the responsibility of the authors and does not necessarily represent the official views of the NIH. Franco Vairoletti is grateful for a fellowship from Agencia Nacional de Investigación e Innovación Uruguay (ANII): ANII (POS_NAC_2018_1_151488). This study was supported by Engineering and Physical Sciences Research Council (grant number EP/M022609/1, Adrian J. Mulholland) and MRC to (grant number MR/T016035/1, Adrian J. Mulholland and James Spencer).

CONFLICT OF INTERESTS

The authors declare no conflict of interest.

PEER REVIEW

The peer review history for this article is available at <https://publons.com/publon/10.1002/prot.26227>.

DATA AVAILABILITY STATEMENT

The underlying data are provided as supplementary information accompanying this paper, or by request from the authors.

ORCID

Silvia Gervasoni  <https://orcid.org/0000-0002-5731-3396>

James Spencer  <https://orcid.org/0000-0002-4602-0571>

Philip Hinchliffe  <https://orcid.org/0000-0001-8611-4743>

Alessandro Pedretti  <https://orcid.org/0000-0001-5916-2029>

Franco Vairoletti  <https://orcid.org/0000-0002-5160-2250>

Graciela Mahler  <https://orcid.org/0000-0003-0612-0516>

Adrian J. Mulholland  <https://orcid.org/0000-0003-1015-4567>

REFERENCES

- WHO, Global Antimicrobial Resistance Surveillance System (GLASS) Report.
- Munita JM, Arias CA. Mechanisms of antibiotic resistance. *Microbiol Spectr*. 2016;4(2):1-34.
- Bush K, Jacoby GA. Updated functional classification of beta-lactamases. *Antimicrob Agents Chemother*. 2010;54(3):969-976.
- Tooke CL, Hinchliffe P, Bragginton EC, et al. β -Lactamases and β -lactamase inhibitors in the 21st century. *J Mol Biol*. 2019;431(18):3472-3500.
- Fritz RA, Alzate-Morales JH, Spencer J, Mulholland AJ, Van Der Kamp MW. Multiscale simulations of Clavulanate inhibition identify the reactive complex in class A β -lactamases and predict the efficiency of inhibition. *Biochemistry*. 2018;57(26):3560-3563.
- Pereira R, Rabelo VWH, Sibajev A, Abreu PA, Castro HC. Class A β -lactamases and inhibitors: in silico analysis of the binding mode and the relationship with resistance. *J Biotechnol*. 2018;279:37-46.
- Tehrani KHME, Martin NI. β -Lactam/ β -lactamase inhibitor combinations: an update. *Medchemcomm*. 2018;9(9):1439-1456.
- Tooke CL, Hinchliffe P, Krajnc A, et al. Cyclic boronates as versatile scaffolds for KPC-2 β -lactamase inhibition. *RSC Med Chem*. 2020;11(4):491-496.
- Mojica MF, Bonomo RA, Fast W. B1-Metallo-beta-lactamases: where do we stand? *Curr Drug Targets*. 2016;17(9):1029-1050.
- Bush K, Bradford PA. Epidemiology of β -lactamase-producing pathogens. *Clin. Microbiol. Rev*. 2020;33(2):e00047-19.
- Rotondo CM, Wright GD. Inhibitors of metallo- β -lactamases. *Curr Opin Microbiol*. 2017;39(11):96-105.
- Lisa MN et al. A general reaction mechanism for carbapenem hydrolysis by mononuclear and binuclear metallo- β -lactamases. *Nat Commun*. 2017;8(1):1-11.
- Meini MR, Llarrull LI, Vila AJ. Overcoming differences: the catalytic mechanism of metallo- β -lactamases. *FEBS Lett*. 2015;589(22):3419-3432.
- Palzkill T. Metallo- β -lactamase structure and function. *Ann N Y Acad Sci*. 2013;1277(1):91-104.
- Laitaoja M, Valjakka J, Jänis J. Zinc coordination spheres in protein structures. *Inorg Chem*. 2013;52(19):10983-10991.
- Li P, Roberts BP, Chakravorty DK, Merz KM. Rational design of particle mesh ewald compatible lennard-jones parameters for +2 metal cations in explicit solvent. *J. Chem. Theory Comput*. 2013;9(6):2733-2748.
- Huggins DJ, Biggin PC, Dämgen MA, et al. Biomolecular simulations: from dynamics and mechanisms to computational assays of biological activity. *Wiley Interdiscip. Rev. Comput. Mol. Sci*. 2019;9(3):e1393.
- Sakharov DV, Lim C. Zn protein simulations including charge transfer and local polarization effects. *J Am Chem Soc*. 2005;127(13):4921-4929.
- Alzahrani KAH, Deeth RJ. Molecular modeling of zinc paddlewheel molecular complexes and the pores of a flexible metal organic framework. *J. Mol. Model*. 2016;22(4):80.
- Peters MB, Yang Y, Wang B, Fusti-Molnar L, Weaver MN, Merz KM. Structural survey of zinc-containing proteins and development of the zinc AMBER force field (ZAFF). *J. Chem. Theory Comput*. 2010;6(9):2935-2947.
- Deeth RJ, Fey N, Williams-Hubbard B. DommiMOE: an implementation of ligand field molecular mechanics in the molecular operating environment. *J Comput Chem*. 2005;26(2):123-130.
- Duarte F, Bauer P, Barrozo A, et al. Force field independent metal parameters using a nonbonded dummy model. *J Phys Chem B*. 2014;118:4351-4362.
- Baker CM. Polarizable force fields for molecular dynamics simulations of biomolecules. *Wiley Interdiscip. Rev. Comput. Mol. Sci*. 2015;5(2):241-254.
- Li P, Merz KM. Metal ion modeling using classical mechanics. *Chem Rev*. 2017;117(3):1564-1686.
- Zuo Z, Liu J. Assessing the performance of the nonbonded Mg^{2+} models in a two-metal-dependent ribonuclease. *J Chem Inf Model*. 2019;59(1):399-408.

26. Pokorná P, Krepl M, Kruse H, Šponer J. MD and QM/MM study of the quaternary HutP homohexamer complex with mRNA, l-histidine ligand, and Mg^{2+} . *J. Chem. Theory Comput.* 2017;13(11):5658-5670.
27. Yu Z, Li P, Merz KM. Extended zinc AMBER force field (EZAFF). *J. Chem. Theory Comput.* 2018;14(1):242-254.
28. Li P, Song LF, Merz KM. Parameterization of highly charged metal ions using the 12-6-4 LJ-type nonbonded model in explicit water. *J Phys Chem B.* 2015;119(3):883-895.
29. Li P, Merz KM. Taking into account the ion-induced dipole interaction in the nonbonded model of ions. *J. Chem. Theory Comput.* 2014;10(1):289-297.
30. Kouda S, Ohara M, Onodera M, et al. Increased prevalence and clonal dissemination of multidrug-resistant *Pseudomonas aeruginosa* with the blaIMP-1 gene cassette in Hiroshima. *J Antimicrob Chemother.* 2009;64(1):46-51.
31. Zhao WH, Hu ZQ. IMP-type metallo- β -lactamases in gram-negative bacilli: distribution, phylogeny, and association with integrons. *Crit Rev Microbiol.* 2011;37(3):214-226.
32. Cornaglia G, Giamarellou H, Rossolini GM. Metallo- β -lactamases: a last frontier for β -lactams? *Lancet Infect Dis.* 2011;11(5):381-393.
33. Gellatly SL, Hancock REW. *Pseudomonas aeruginosa*: new insights into pathogenesis and host defenses. *Pathog Dis.* 2013;67(3):159-173.
34. Nguyen L, Garcia J, Gruenberg K, MacDougall C. Multidrug-resistant pseudomonas infections: hard to treat, but Hope on the horizon? *Curr. Infect. Dis. Rep.* 2018;20(8):23.
35. Ju LC, Cheng Z, Fast W, Bonomo RA, Crowder MW. The continuing challenge of Metallo- β -lactamase inhibition: mechanism matters. *Trends Pharmacol Sci.* 2018;39(7):635-647.
36. Tehrani KHME, Martin NI. Thiol-containing metallo- β -lactamase inhibitors resensitize resistant gram-negative bacteria to meropenem. *ACS Infect Dis.* 2017;3:711-717.
37. Klingler FM, Wichelhaus TA, Frank D, et al. Approved drugs containing thiols as inhibitors of metallo- β -lactamases: strategy to combat multidrug-resistant bacteria. *J Med Chem.* 2015;58(8):3626-3630.
38. Brem J, Van Berkel SS, Zollman D, et al. Structural basis of metallo- β -lactamase inhibition by captopril stereoisomers. *Antimicrob Agents Chemother.* 2016;60(1):142-150.
39. Rossi M-A, Martinez V, Hinchliffe P, et al. 2-Mercaptomethylthiazolidines use conserved aromatic-S interactions to achieve broad-range inhibition of metallo- β -lactamases. *Chem Sci.* 2021;12:2898-2908.
40. Pavlin M, Rossetti G, De Vivo M, Carloni P. Carnosine and Homocarnosine degradation mechanisms by the human carnosinase enzyme CN1: insights from multiscale simulations. *Biochemistry.* 2016;55(19):2772-2784.
41. Korb O, Stützel T, Exner TE. An ant colony optimization approach to flexible protein-ligand docking. *Swarm Intell.* 2007;1:115-134.
42. Korb O, Stützel T, Exner TE. PLANTS: application of ant Colony optimization to structure-based drug design. *Lecture Notes in Computer Science.* Springer; 2006:247-258.
43. Salomon-Ferrer R, Case DA, Walker RC. An overview of the Amber biomolecular simulation package. *Wiley Interdiscip Rev Comput Mol Sci.* 2013;3(2):198-210.
44. Case DA, Wang J, Wolf RM, Caldwell JW, Kollman PA. Development and testing of a general amber force field. *J Comput Chem.* 2004;25:1157-1174.
45. Mobley DL, Lim VT, Hahn DF, Tresadern G, Bayly CI. Benchmark assessment of molecular geometries and energies from small molecule force fields. *F1000Research.* 2020;9:1390.
46. Maier JA, Martinez C, Kasavajhala K, Wickstrom L, Hauser KE, Simmerling C. ff14SB: improving the accuracy of protein side chain and backbone parameters from ff99SB. *J. Chem. Theory Comput.* 2015;11:3696-3713.
47. Kräutler V, Van Gunsteren WF, Hünenberger PH. A fast SHAKE algorithm to solve distance constraint equations for small molecules in molecular dynamics simulations. *J Comput Chem.* 2001;22(5):501-508.
48. Gaus M, Cui Q, Elstner M. DFTB3: extension of the self-consistent-charge density-functional tight-binding method (SCC-DFTB). *J. Chem. Theory Comput.* 2011;7(4):931-948.
49. Lonsdale R, Harvey JN, Mulholland AJ, Lonsdale R. A practical guide to modelling enzyme-catalysed reactions. *Chem Soc Rev.* 2012;41:3025-3038.
50. Cui Q, Elstner M. Density functional tight binding: values of semi-empirical methods in an ab initio era. *Phys Chem Chem Phys.* 2014;16(28):14368-14377.
51. ChemShell, A computational chemistry shell. www.chemshell.org.
52. Todorov IT, Smith W, Trachenko K, Dove MT. DL_POLY_3: new dimensions in molecular dynamics simulations via massive parallelism. *J Mater Chem.* 2006;16(20):1911-1918.
53. Grimme S. Semiempirical GGA-type density functional constructed with a long-range dispersion correction. *J Comput Chem.* 2006;27(15):1787-1799.
54. Lonsdale R, Harvey JN, Mulholland AJ. Effects of dispersion in density functional based quantum mechanical/molecular mechanical calculations on cytochrome P450 catalyzed reactions. *J Chem Theory Comput.* 2012;8(11):4637-4645.
55. Chaskar P, Zoete V, Röhrig UF. Toward on-the-fly quantum mechanical/molecular mechanical (QM/MM) docking: development and benchmark of a scoring function. *J Chem Inf Model.* 2014;54(11):3137-3152.
56. Trott O, Olson AJ. AutoDock Vina: improving the speed and accuracy of docking with a new scoring function, efficient optimization and multithreading. *J Comput Chem.* 2010;31(2):455-461.
57. Korb O, Stützel T, Exner TE. Empirical scoring functions for advanced protein-ligand docking with plants. *J Chem Inf Model.* 2009;49:84-96.
58. Concha NO, Janson CA, Rowling P, et al. Crystal structure of the IMP-1 metallo β -lactamase from *Pseudomonas aeruginosa* and its complex with a mercaptocarboxylate inhibitor: binding determinants of a potent, broad-spectrum inhibitor. *Biochemistry.* 2000;39(15):4288-4298.
59. Kurosaki H, Yamaguchi Y, Higashi T, et al. Irreversible inhibition of metallo- β -lactamase (IMP-1) by 3-(3-mercaptopropionylsulfanyl) propionic acid pentafluorophenyl Ester. *Angew Chemie Int Ed.* 2005;44(25):3861-3864.
60. Kurosaki H, Yamaguchi Y, Yasuzawa H, Jin W, Yamagata Y, Arakawa Y. Probing, inhibition, and crystallographic characterization of metallo- β -lactamase (IMP-1) with fluorescent agents containing dansyl and thiol groups. *ChemMedChem.* 2006;1(9):969-972.
61. Hinchliffe P, González MM, Mojica MF, et al. Cross-class metallo- β -lactamase inhibition by bisthiazolidines reveals multiple binding modes. *Proc Natl Acad Sci U S A.* 2016;113(26):E3745-E3754.
62. de Arruda EGR, Rocha BA, Barrionuevo MVF, et al. Zn (II) coordination sphere and chemical structure influence over the reactivity of metallo- β -lactamase model compounds. *Dalt Trans.* 2018;48(9):2900-2916.
63. Martin DP, Blachly PG, Mccammon JA, Cohen SM. Exploring the influence of the protein environment on metal-binding pharmacophores. *J Med Chem.* 2014;57:7126-7135.
64. Kapusta DP, Firsov DA, Khrenova MG, Grigorenko BL, Nemukhin AV. Effect of solvation water shells on enzyme active sites in zinc-dependent hydrolases. *Struct Chem.* 2019;30(2):481-488.
65. Concha NO, Rasmussen BA, Bush K, Herzberg O. Crystal structure of the wide-spectrum binuclear zinc β -lactamase from *Bacteroides fragilis*. *Structure.* 1996;4(7):823-836.
66. Lu X, Gaus M, Elstner M, Cui Q, Festschrift WLJ. Parametrization of DFTB3/3OB for magnesium and zinc for chemical and biological applications the traditional semiempirical QM methods based on the neglect-of-diatomic-differential-overlap (NDDO) approxima-special issue. *J Phys Chem B.* 2015;119:45.

67. Chakravorty DK, Wang B, Lee CW, Giedroc DP, Merz KM. Simulations of allosteric motions in the zinc sensor CzrA. *J Am Chem Soc.* 2012;134(7):3367-3376.
68. Vidossich P, Magistrato A. QM/MM molecular dynamics studies of metal binding proteins. *Biomolecules.* 2014;4(3):616-645.
69. Wu S, Xu D, Guo H. QM/MM studies of Monozinc b-lactamase CphA suggest that the crystal structure of an enzyme-intermediate complex represents a minor pathway. *J Am Chem Soc.* 2010;132:17986-17988.
70. Khrenova MG, Nemukhin AV. Modeling the transient kinetics of the L1 metallo- β -lactamase. *J Phys Chem B.* 2018;122(4):1378-1386.
71. Huntley JJA, Fast W, Benkovic SJ, Wright PE, Dyson HJ. Role of a solvent-exposed tryptophan in the recognition and binding of antibiotic substrates for a metallo- β -lactamase. *Protein Sci.* 2003;12:1368-1375.
72. Moali C, Anne C, Lamotte-Brasseur J, et al. Analysis of the importance of the metallo- β -lactamase active site loop in substrate binding and catalysis. *Chem Biol.* 2003;10(4):319-329.
73. Montagner C, Nigen M, Jacquin O, et al. The role of active site flexible loops in catalysis and of zinc in conformational stability of *Bacillus cereus* 569/H/9 β -lactamase. *J Biol Chem.* 2016;291(31):16124-16137.
74. Meini MR, Llarrull LI, Vila AJ. Evolution of metallo- β -lactamases: trends revealed by natural diversity and in vitro evolution. *Antibiotics.* 2014;3(3):285-316.
75. Salmaso V, Moro S. Bridging molecular docking to molecular dynamics in exploring ligand-protein recognition process: an overview. *Front Pharmacol.* 2018;9:923.
76. Amaro RE, Baudry J, Chodera J, et al. Ensemble docking in drug discovery. *Biophys J.* 2018;114(10):2271-2278.
77. Ge Y, van der Kamp M, Malaisree M, Liu D, Liu Y, Mulholland AJ. Identification of the quinolinedione inhibitor binding site in Cdc25 phosphatase B through docking and molecular dynamics simulations. *J Comput Aided Mol Des.* 2017;31(11):995-1007.
78. Irwin JJ, Raushel FM, Shoichet BK. Virtual screening against metalloenzymes for inhibitors and substrates. *Biochemistry.* 2005;44(37):12316-12328.
79. Pecina A, Haldar S, Fanfrlík J, et al. SQM/COSMO scoring function at the DFTB3-D3H4 level: unique identification of native protein-ligand poses. *J Chem Inf Model.* 2017;57(2):127-132.
80. Pecina A, Meier R, Fanfrlík J, et al. The SQM/COSMO filter: reliable native pose identification based on the quantum-mechanical description of protein-ligand interactions and implicit COSMO solvation. *Chem Commun.* 2016;52(16):3312-3315.
81. Mamatkulov S, Schwierz N. Force fields for monovalent and divalent metal cations in TIP3P water based on thermodynamic and kinetic properties. *J. Chem. Phys.* 2018;148(7):074504.
82. Fracchia F, Del Frate G, Mancini G, Rocchia W, Barone V. Force field parametrization of metal ions from statistical learning techniques. *J. Chem. Theory Comput.* 2018;14(1):255-273.
83. Z. Jing, R. Qi, C. Liu, and P. Ren, "Study of interactions between metal ions and protein model compounds by energy decomposition analyses and the AMOEBA force field," *J. Chem. Phys.*, vol. 147, no. 16, p. 161733, 2017.
84. Çınaroglu SS, Timuçin E. Comparative assessment of seven docking programs on a nonredundant metalloprotein subset of the PDB bind refined. *J Chem Inf Model.* 2019;59(9):3846-3859.
85. Corbeil CR, Williams CI, Labute P. Variability in docking success rates due to dataset preparation. *J Comput-Aid Mol Des.* 2012;26(6):775-786.
86. Oelschlaeger P, Schmid RD, Pleiss J. Insight into the mechanism of the IMP-1 metallo- β -lactamase by molecular dynamics simulations. *Protein Eng Des Sel.* 2003;16(5):341-350.
87. Hinchliffe P, Tanner CA, Krismanich AP, et al. Structural and kinetic studies of the potent inhibition of metallo- β -lactamases by 6-phosphonomethylpyridine-2-carboxylates. *Biochemistry.* 2018;57(12):1880-1892.
88. Bergonzo C, Hall KB, Cheatham TE. Divalent ion dependent conformational changes in an RNA stem-loop observed by molecular dynamics. *J. Chem. Theory Comput.* 2016;12(7):3382-3389.

SUPPORTING INFORMATION

Additional supporting information may be found in the online version of the article at the publisher's website.

How to cite this article: Gervasoni S, Spencer J, Hinchliffe P, et al. A multiscale approach to predict the binding mode of metallo beta-lactamase inhibitors. *Proteins.* 2021;1-13. doi: 10.1002/prot.26227